Comparison of Acceleration Methods in a Radiation Transport Code With Adaptive Mesh Refinement

Carlos García-Fernández, Pedro Velarde, and Manuel Cotelo

***Abstract*—New considerations about the acceleration of an iterative process to couple the radiation transport equation and the equation of matter temperature are presented in this paper. Two synthetic acceleration methods [diffusion synthetic acceleration (DSA) and transport synthetic acceleration (TSA)] have been studied and analyzed, showing its strengths and weaknesses. This study is applied to an adaptive mesh refinement (AMR) context, concluding in a better performance of DSA for coarse level resolutions with higher S_n, while TSA is better for finer level boxes and smaller S_n cases. These conclusions are applied to accelerate the resolution of an AMR problem.**

***Index Terms*—Adaptive mesh refinement (AMR), diffusion synthetic acceleration (DSA), radiation transport, synthetic acceleration, transport synthetic acceleration (TSA).**

I. Introduction

IN A NUMBER of different problems involving high-energy density plasmas, such as those presented in ICF or laboratory astrophysics, radiation plays a relevant role, which has to be taken into account in hydrodynamic simulations in order to obtain reliable results. To do that, the equations governing the radiation transport coupled with matter have to be solved into the hydro code. These equations, neglecting scattering and matter conduction, can be written [1]

$$\left(\frac{1}{c}\frac{\partial}{\partial t}+\mathbf{\Omega}\cdot\boldsymbol{\nabla}\right)I=\sigma_a(B-I) \tag{1}$$

$$\frac{1}{c}c_v(T)\frac{\partial T}{\partial t}=\int_0^\infty \sigma_a^\nu\left(\int_{\mathbf{\Omega}} I d\mathbf{\Omega}-B\right)d\nu \tag{2}$$

where $I(\mathbf{x},\mathbf{\Omega},\nu,t)$ is the specific radiation intensity, $B(\mathbf{x},T,\nu,t)$ is the matter emissivity, T is the matter temperature, $\sigma_a(\mathbf{x},T,\nu,t)$ is the absorption coefficient, $c_v(T)$ is the volumetric heat capacity, and $\mathbf{\Omega}$ is the solid angle. Since I depends upon seven variables (three of space, two of direction, one of frequency, and one of time) and B presents a nonlinear dependence on matter temperature, these equations are very time consuming to solve, even more when they are coupled with hydrodynamics.

For that reason, it is necessary to look for approximations that allow to solve the problem with a reasonable accuracy without being too expensive in terms of computational execution time.

There is a wide range of approximations that can be found in literature [2]. The simplest technique to deal with this problem is the diffusion model, which neglects the angular dependence of the equations, but this approximation has the drawback that it is invalid for cases where anisotropy is important. For that reason, many methods have been created to treat the angular dependence. Among them, the most commonly used are the spherical harmonics (P_n) method [3], which expands the angular intensity in a truncated series of Legendre polynomials, denoting the subscript n as the order of the expansion, and the discrete-ordinate (S_n) method [4], in which the solid angle is discretized into several directions that are solved independently, being n related to the number of directions and, hence, with the accuracy of the approximation. This latter method, which will be employed in this paper, transforms (1) in a set of equations (one for each direction), where the angular dependence has been eliminated. Therefore, it has the advantage of treating accurately cases with strong angular dependence, but its resolution time can be very large since it implies the resolution of many equations, increasing when the order of S_n approximation grows. For that reason, any improvement in the execution speed is of crucial significance.

In this paper, we are going to evaluate two methods to accelerate the convergence of iterations carried out to couple the radiation equation with matter. First, in Section II, we will present the environment of the radiation transport solver [5], the hydrodynamic code ARWEN. Later, in Section III, the coupling with matter and its problematic will be presented, as well as the foundations of the synthetic acceleration methods. In the next sections, a Fourier analysis will be carried out, and finally, both methods will be applied to the solution of an academic and a real adaptive mesh refinement (AMR) problem.

II. ARWEN Code

All the calculations carried out in this paper have been done in the frame of ARWEN code [6], which is a code designed to solve problems of fluids at high temperature and density that has been applied in different problems in ICF, astrophysics, and X-ray lasers [7]. To do that, it solves the compressible fluid dynamics equations with electron conduction and radiation transport. All these calculations are done in an AMR context.

Manuscript received December 1, 2009; revised April 29, 2010 and May 24, 2010; accepted May 28, 2010. Date of publication July 15, 2010; date of current version September 10, 2010. This work was supported in part by the European Commission Projects HiPER-PP (211737) and ELI-PP (212105), by the Spanish MEC Program ENE2009-09837/FTN, and by the Comunidad de Madrid (ESF).

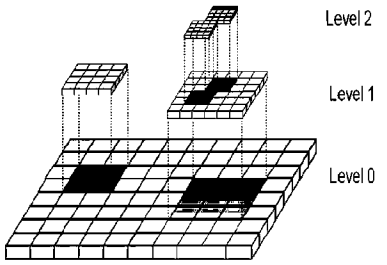

Fig. 1. Two-dimensional AMR hierarchical tree with two levels of refinement.

AMR [8] is a numerical technique consisting in refining locally in the zones where the numerical error is bigger by adding new meshes with higher refinement. This leads to a homogeneous error in the whole domain. By doing that, the problem, instead of having a uniform mesh, presents a set of AMR meshes structured in a hierarchical tree, as shown in Fig. 1, involving different levels of spatial refinement that have to be solved sequentially.

The AMR radiation transport solver presented in this paper is integrated into ARWEN, where it is coupled with other modules such as hydrodynamics or thermal conduction, in order to solve completely a high-energy density plasma problem. The kernel of its calculations has been extracted from PARTISN [9], as well as the implementations of diffusion synthetic acceleration (DSA) [10] and transport synthetic acceleration (TSA) methods. The details about the resolution of different levels and the transmission of data between meshes can be found in [6].

III. Synthetic Acceleration

In high-energy density plasma problems, radiation has to be solved coupled with matter. In order to treat the frequency dependence, the spectrum is divided into G groups of energy, where each variable is integrated. Using this multigroup approximation, (1) and (2) have the following aspect for each group g:

$$\left(\frac{1}{c}\frac{\partial}{\partial t} + \mathbf{\Omega}\cdot\boldsymbol{\nabla} + \sigma_{t,g}\right) I_g = \sigma_{t,g} B_g(T) \tag{3}$$

$$\frac{1}{c} c_v \frac{\partial T}{\partial t} = \sum_{g=1}^{G} \sigma_{t,g} \left(\int I_g d\mathbf{\Omega} - B_g(T)\right) \tag{4}$$

where I_g is the radiation intensity in the group, $\sigma_{t,g}$ is the total cross section in the group, and B_g is the Planck function integrated over the group, assuming local thermodynamic equilibrium conditions.

To deal with the nonlinear dependence of the temperature, the Planckian can be approximated by this formula

$$B_g(T) = B_g(T_0) + (T - T_0)\frac{\partial B_g(T_0)}{\partial T} \tag{5}$$

and replaced in (3) and (4). Using a similar formalism as in [11] and [12] and a backward Euler discretization in time, the expression obtained is as follows:

$$\left(\frac{1}{c\Delta t} + \mathbf{\Omega}\cdot\boldsymbol{\nabla} + \sigma_{t,g}\right) I_g = \frac{\eta}{4\pi}\sum_{g=1}^{G}\chi_g\sigma_{t,g}\phi_g + S_g \tag{6}$$

where

$$\chi_g = \frac{\sigma_{t,g}\frac{\partial B_g(T_0)}{\partial T}}{\sum_{g=1}^{G}\sigma_{t,g}\frac{\partial B_g(T_0)}{\partial T}} \tag{7}$$

$$\phi_g = \int I_g d\mathbf{\Omega} \tag{8}$$

$$\eta = \frac{\sum_{g=1}^{G}\sigma_{t,g}\frac{\partial B_g(T_0)}{\partial T}}{\frac{c_v}{4\pi\Delta t} + \sum_{g=1}^{G}\sigma_{t,g}\frac{\partial B_g(T_0)}{\partial T}} \tag{9}$$

$$S_g = \frac{I_g^0}{c\Delta t} + \sigma_{t,g}B_g(T_0) + \eta\chi_g\sum_{g'=1}^{G}\sigma_{g'}B_{g'}(T_0) \tag{10}$$

and I_g^0 is the intensity of the previous time step. It is important to note that, in this case, one can establish a relation between the $\eta\chi_g\sigma_{t,g}$ term and a scattering cross section, since both equations would be algebraically similar. The main difficulty in the resolution of (6) is the estimation of the value of the scalar flux ϕ_g, since it consists in an integral of the radiation intensity in all directions. There is a wide range of methods to deal with this problem that can be found in literature [13]. In this paper, we will study the performance of three of them: source iteration (SI), DSA, and TSA.

A. SI

It is the most simple method to find the solution. It consists just in solving (6) by estimating ϕ_g from the data of the previous iteration. The process to calculate I_g^{l+1} would just require to solve, for each frequency group g, the following equation:

$$\left(\frac{1}{c\Delta t} + \mathbf{\Omega}\cdot\boldsymbol{\nabla} + \sigma_{t,g}\right) I_g^{l+1} = \frac{\eta}{4\pi}\sum_{g=1}^{G}\chi_g\sigma_{t,g}\phi_g^l + S_g \tag{11}$$

where

$$\phi_g^l = \int I_g^l d\mathbf{\Omega} \tag{12}$$

and by integrating I_g^{l+1}, the scalar flux ϕ_g^{l+1} can be obtained for the next iteration. Although this is the less expensive method in terms of computational execution time per iteration, this method has been shown to have a too slow convergence rate in cases where the ratio

$$\xi = \frac{\eta\chi_g\sigma_{t,g}}{\sigma_{t,g} + \frac{1}{c\Delta t}} \tag{13}$$

is close to one. For that reason, it is necessary to use methods to speed up the convergence rate, such as DSA or TSA, among many others.

B. DSA

The DSA method [14] proposes the use of a diffusion equation, consistently discretized, as a low-order operator for the problem, keeping the SI step as high-order operator.

The iteration process in each group g consists in the following three steps.

1) An SI step is carried out, solving (11) to obtain $I_g^{l+1/2}$ and using (12) $\phi_g^{l+1/2}$.
2) Then, the following diffusion equation has to be solved:

$$\nabla\cdot\left(\frac{1}{3\sigma_{t,g}}\nabla R_g^{l+1}\right)+\sigma_{t,g}R_g^{l+1}=\eta\chi_g\sigma_{t,g}\left(\phi_g^{l+1/2}-\phi_g^{l}\right) \quad (14)$$

3) The scalar flux for the next iteration is updated: $\phi_g^{l+1}=\phi_g^{l+1/2}+R_g^{l+1}$.

This method overcomes the difficulties presented in the SI method in cases in which the convergence rate is low. The main disadvantages are that an extra time has to be spent in solving the diffusion equation and also that the diffusion and transport equations have to be discretized consistently. Moreover, DSA degrades also in problems with material discontinuities [15].

C. TSA

The TSA method was proposed in [16] as a development of the previous S_2SA developed by Larsen and Miller [17], who use an S_2 transport equation as an accelerator. Unlike S_2SA method, TSA can be used in multidimensional geometries by keeping part of the scattering term (in this case, $\eta\chi_g\sigma_{t,g}$) in the low-order operator introducing the parameter β in the transport equation. By doing this, the low-order operator has a scattering term given by $(1-\beta)\eta\chi_g\sigma_{t,g}$.

The basic scheme of the iteration in TSA in each group g is the following.

1) As a high-order operator, $I_g^{l+1/2}$ and $\phi_g^{l+1/2}$ are obtained from an SI step ((11) is solved).
2) As a low-order operator, a discrete-ordinate equation is used. This equation can be written, using the same notation as in [16]

$$\begin{aligned}\mathbf{\Omega}\cdot\nabla f_g^{l+1,r}+(1-\beta\eta\chi_g)\sigma_{t,g}f_g^{l+1,r}\\ =\frac{(1-\beta)\eta\chi_g\sigma_{t,g}}{4\pi}F_g^{l+1,r-1}+\frac{\eta\chi_g\sigma_{t,g}}{4\pi}\left(\phi_g^{l+1/2}-\phi_g^{l}\right)\end{aligned} \quad (15)$$

where

$$F_g^{l+1,r-1}=\int f_g^{l+1,r-1}d\mathbf{\Omega} \quad (16)$$

and $F_g^{l+1,0}$ is set to zero in the first iteration. This problem is similar to those presented in (11) and can be solved by developing an SI iterative process denoted by the r index. The main difference is that the S_n^{TSA} order employed to solve (15) is usually small, S_2 or S_4, in order to make this step not too expensive in terms of resolution time. In practice, it is usual to set a maximum number of iterations N_{it} in the SI method to solve (15). Although this does not allow a full convergence of the low-order equation in many cases, it has been shown that an adequate value of N_{it} can reduce dramatically the overall computational cost of the method [16]. Therefore, the choice of β and N_{it} is crucial for a good performance of this method.
3) The scalar flux is updated by doing $\phi^{l+1}=\phi^{l+1/2}+F_g^{l+1}$.

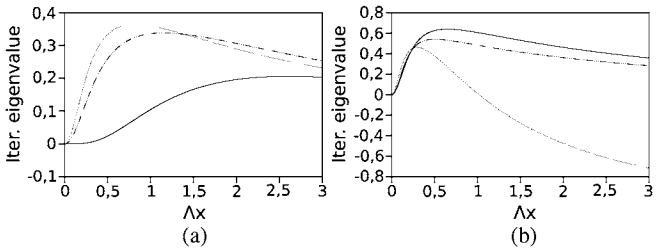

Fig. 2. Iteration eigenvalues for (a) DSA and (b) TSA as functions of Λ_x using different Λ_y/Λ_x ratios: (Solid line) 0, (line–dotted line) 0.5, and (dotted line) 1 using the default conditions defined in the text.

This method has also a faster convergence than SI, and it is easier to implement than a DSA method in a transport code because the solution procedure for the high- and low-order equations will be the same as both are transport equations. However, solving a transport equation usually implies a large computational cost, which increases with S_n^{TSA} order; thus, the acceleration has to compensate the extra cost of the new low-order operator.

IV. Fourier Analysis

To evaluate the convergence and the efficiency of the methods, the theoretical tool that will be employed is the Fourier analysis. For simplicity, we will consider an infinite medium with constant cross section, which has been shown to be a good approximation for the study of synthetic acceleration methods. The calculation of the iteration eigenvalues for SI, DSA, and TSA and the assumptions taken are shown in the Appendix. The expressions obtained for the eigenvalues are (32), (36), and (51), respectively. All expressions are periodic for the Fourier modes $\lambda_x\in[0,2\pi/\sigma_t\Delta x]$ and $\lambda_y\in[0,2\pi/\sigma_t\Delta y]$.

The first crucial point would be to examine the analytical expressions for the iteration eigenvalues obtained and where they reach their maximum and minimum values, which will determine the spectral radius of the iterations. From these equations, the following conclusions can be obtained.

1) According to the expression of the iteration eigenvalue ω_{SI} given in (32), the SI method has its worst performance for the flat mode ($\lambda_x=\lambda_y=0$) when $\omega_{\mathrm{SI}}=\xi$. This is particularly problematic when ξ is near one, because this will cause a too slow convergence.
2) Since the expression of the eigenvalue of the DSA method ω_{DSA} depends on Λ_x and Λ_y defined in (33) and (34), we have shown the curves for different Λ_x/Λ_y ratios in Fig. 2(a). It is shown that it reaches the largest spectral radius when this ratio is one, i.e., in diagonal modes. The stability of the method is guaranteed since $\omega_{\mathrm{DSA}}<\xi$ in all modes, as shown in [14].

TABLE I
ρ^+ AND ρ^- FOR TSA AS A FUNCTION OF LOW-ORDER S_n^{TSA} AND β. HIGH-ORDER $S_n = S_8$ AND $\xi = 0.9$. $\Delta x = \Delta y = 10^{-3}$

	$\beta = 0.1$		$\beta = 0.5$		$\beta = 0.9$	
	ρ^+	ρ^-	ρ^+	ρ^-	ρ^+	ρ^-
S_2^{TSA}	0.552	0.715	0.638	1.15	0.755	2.07
S_4^{TSA}	0.446	0.082	0.518	0.188	0.662	0.678

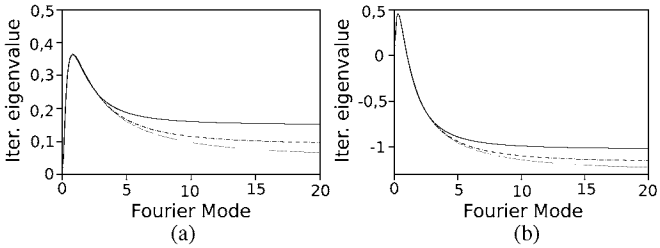

Fig. 3. Iteration eigenvalues for (a) DSA and (b) TSA using (solid line) S_6, (line–dotted line) S_{10}, and (dotted line) S_{14}.

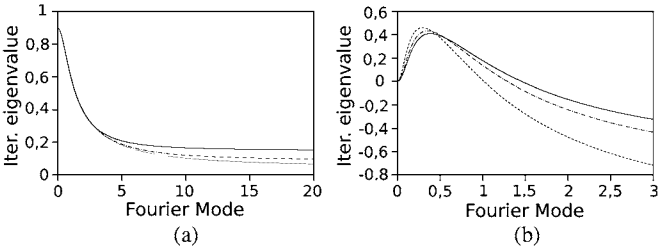

Fig. 4. (a) Eigenvalues for different SIs using (solid) S_6, (line–dotted line) S_{10}, and (dotted line) S_{14}. (b) Results for (dotted line) $\beta = 1$, (line–dotted line) $\beta = 0.7$, and (solid line) $\beta = 0.5$ in TSA.

3) From the study of (51) that defines the iteration eigenvalue ω_{TSA}, it can be concluded that it reaches its most positive (ρ^+) value in the 1-D modes (when λ_x or λ_y is zero), while its most negative values (ρ^-) are found in diagonal modes ($\lambda_x = \lambda_y$). This conclusions can be observed in Fig. 2(b), where it has been represented ω_{TSA} for different Λ_x/Λ_y ratios. To study the influence of S_n^{TSA} and β, the values of ρ^+ and ρ^- are represented in Table I for different combinations of these parameters. It can be seen that, for large β values, an S_2 discretization can be unstable, while for S_4, it remains stable, which is a fact already presented in [16] in a more general analysis.

Since ω_{SI}, ω_{DSA}, and ω_{TSA} depend upon many factors (Fourier modes λ_x and λ_y, σ_t, ξ, and S_n among others), the iteration eigenvalues have been represented as a function of the Fourier modes, changing the other parameters in order to evaluate its influence on the iterative process, as can be seen in Figs. 3–6. For these eigenvalue calculations, we have chosen as default data $\sigma_t = 1$, $\Delta x = \Delta y = 10^{-3}$, $S_n^{\mathrm{TSA}} = 2$, $\beta = 0.5$, $\xi = 0.9$, $\lambda_x = \lambda_y = \lambda$, and $S_n = 8$, unless anything different is said in the figure. Lastly, in the discrete-ordinate equations, a level symmetric quadrature has been used for the angular discretization. The following conclusions can be reached in the light of these figures.

1) In Figs. 3(a) and (b) and 4(b), it has been represented that the results for SI, DSA, and TSA with three different S_n orders (S_6, S_{10}, and S_{14}). For low Fourier modes, the curves overlap, but for high values, they reach different asymptotic values. While the maximum eigenvalues of SI and DSA remain unaffected when the S_n order increases, TSA improves its convergence for small S_n.

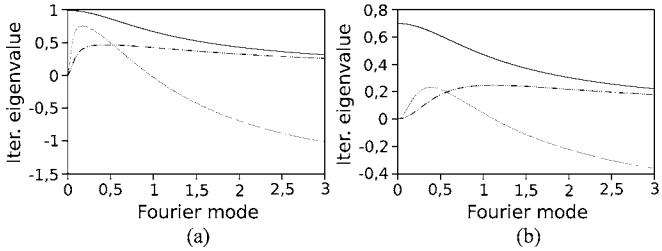

Fig. 5. Eigenvalues for different values of ξ's for (solid line) SI, (line–dotted line) DSA, and (dotted line) TSA. (a) Eigenvalue for $\xi = 0.99$. (b) Eigenvalue for $\xi = 0.7$.

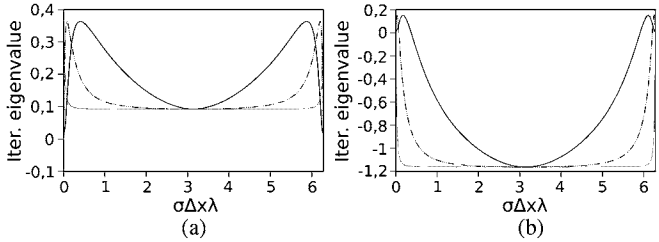

Fig. 6. Iteration eigenvalues using (solid) $\Delta x = 0.5$, (line–dotted line) $\Delta x = 0.1$, and (dotted line) $\Delta x = 0.01$ for (a) DSA and (b) TSA in function of $\sigma \Delta x \lambda$.

2) From Fig. 5, it can be observed that the closer to one is ξ, the worse is the performance of the TSA and SI methods, whereas DSA has well-bounded values of eigenvalues in both cases.
3) The eigenvalues of TSA improve by decreasing β down to 0.5. For smaller values, the curve reaches an asymptotic value. This result was already presented in [16].
4) The spatial discretization Δx and Δy does not have a significant influence on the stability of the methods from the Fourier analysis point of view. The spectral radius of SI method is always given by the value of ξ for $\lambda = 0$, independently of the mesh used. In both DSA and TSA methods, a change in the spatial mesh does not affect the maximum and minimum eigenvalues, as can be inferred from Fig. 6, where the eigenvalues have been represented for a period $\lambda \in [0, 2\pi/\sigma_t \Delta x]$.

V. NUMERICAL RESULTS

A. 2-D Academic Test

In order to test the performance of the methods, we have first considered a classical 2-D problem with an isotropic incoming boundary flux condition on the left bound. This kind of problems has been widely used to test these methods.

The conditions used are the following.

1) We do not consider any interaction with matter. Instead of that, we will solve a stationary radiation problem with scattering in one group, which is formally identical to the problem of coupling with matter. This will make easier to

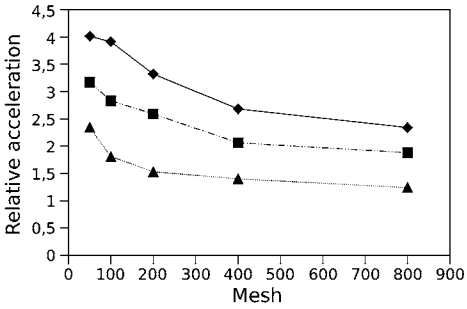

Fig. 7. Relative acceleration for different meshes with $\xi = 0.9$ for (solid line) S_{14}, (line–dotted line) S_{10}, and (dotted line) S_6.

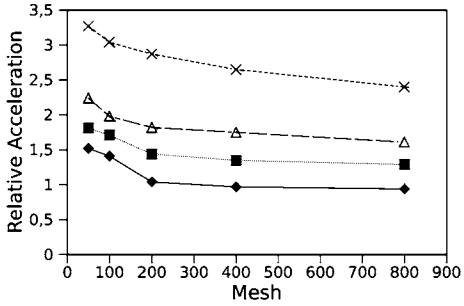

Fig. 8. Relative acceleration with S_8 as a function of mesh size for (short line) $\xi = 0.99$, (long line) $\xi = 0.9$, (dotted line) $\xi = 0.7$, and (solid line) $\xi = 0.5$.

TABLE II
HIGH-ORDER ITERATIONS FOR TSA IN FUNCTION OF NUMBER OF MESHES AND σ_t (cm^{-1})

Nr. meshes	50	100	200	400	800
$\sigma_t = 0.1$	12	12	11	11	11
$\sigma_t = 1$	74	68	63	60	60
$\sigma_t = 10$	138	122	109	103	98

TABLE III
EXECUTION TIME (IN SECONDS) AND NUMBER OF ITERATIONS FOR THE HIGH-ORDER EQUATION IN TSA FOR $\xi = 0.99$

	$\beta = 0.2$		$\beta = 0.5$		$\beta = 0.9$	
	Ex. time	Iters.	Ex. time	Iters.	Ex. time	Iters.
N_{it}=2	285.2	187	318.1	206	368.1	239
N_{it}=5	250	129	351.4	180	417.7	238
N_{it}=10	273.2	107	408.9	174	432.5	238
N_{it}=∞	452.4	101	460.1	174	433.6	238
SI	Ex. time= 505.2 s. It=441					

evaluate the results, as the scattering cross section is an input datum.

2) The medium will be homogeneous with $\sigma_t = 1$ cm^{-1} and a dimension of 40 $\times$ 40 cm. Doing this, the scattering cross section (σ_s) is equivalent to ξ parameter in this problem.
3) The boundary conditions will be free, i.e., no incoming photons, for the rest of the boundaries.
4) The incoming flux will be a blackbody radiation of 40 eV.
5) In order to solve the linear system given by the diffusion equation of DSA method, a conjugate gradient method has been used.
6) In the TSA method, to solve the low-order equation, an S_2 level symmetric quadrature set has been employed, and N_{it} has been set to five. To solve the discrete-ordinate equation, a diagonal plane sweep implemented in PARTISN has been employed.

The variables that will be evaluated are the S_n order, ξ, and σ_t, all of them studied as a function of the mesh size. To compare the performances of both methods, we will represent the relative acceleration, i.e., the TSA execution time divided by the DSA one.

First, we represent the results obtained for different S_n orders in Fig. 7. Two conclusions can be extracted: First, the performance of TSA improves when the mesh size is refined, and second, when S_n order is smaller, TSA acceleration improves its result in comparison to DSA. The worse performance of TSA method for the cases with high optical thickness ($\sigma_t \Delta x$) was already anticipated in [16] for a different spatial discretization method. In order to evaluate this influence, in Table II, the number of high-order iterations required to converge as a function of the total cross section σ_t has been measured. One can conclude from the data that the larger the $\sigma_t \Delta x$ is, the slower is the convergence of the method.

The influence of ξ is evaluated in Fig. 8. It can be observed that, for low values of the parameter, TSA is even better than DSA. However, for ξ near one (when acceleration is more required), the performance of TSA gets dramatically worse compared with DSA.

Lastly, an analysis of the influence of β and the maximum number of iterations permitted to solve the low-order equation of TSA (N_{it}) has been developed and its results shown in Table III. The important time saving that is achieved by TSA in comparison to SI, specially by choosing a $\beta < 0.5$, can be clearly seen. Moreover, two conclusions can be inferred from these results: First, using a high N_{it} does not make any sense in many cases, since it just increases the time employed in solving the low-order equation without achieving a reduction of the number of iterations required for the high-order one, producing an increase in the total execution time. The second conclusion is that the optimal choice of N_{it} depends on the choice of β. For low β, it is better to use a higher N_{it}, whereas in high β cases, a low N_{it} decreases the computational execution time. This is because a low β produces a slow convergence of low-order equation but a faster convergence of the high-order one, while for high β, the contrary happens.

B. Application to a Laser-Created Plasma

As an application of what has been exposed previously, we have used TSA and DSA methods in the resolution of a simulation case in AMR using the ARWEN code. In order to deal with an interesting case to evaluate the performance of the methods, we have chosen a simulation in which the parameter ξ is near one. In one group, this parameter can be written in the following form:

$$\xi = \left(1 + \frac{c_v}{16\pi a \sigma_t T^3 \Delta t}\right)^{-1}. \tag{17}$$

Thus, we deal with a case when $\sigma_t T^3 \Delta t \gg 0$. This means that acceleration will have a relevant role in high-temperature cases within a highly absorbent medium.

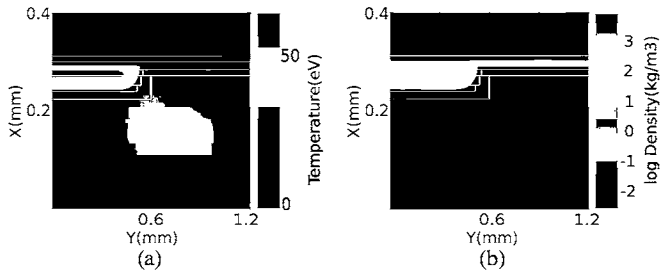

Fig. 9. Density and temperature for iron plasma after 1.2 ns. (a) Electron temperature. (b) Density.

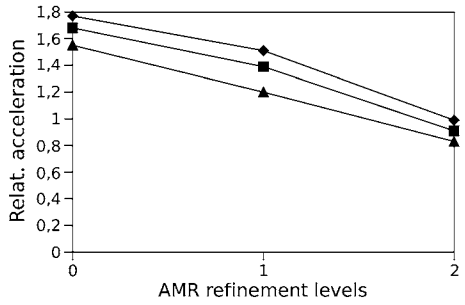

Fig. 10. Relative acceleration TSA versus DSA for (triangles) S_6, (squares) S_{10}, and (diamonds) S_{14}.

To evaluate the performance of the methods, we have chosen an iron laser-created plasma inspired in [18]. It consists in a 1-ns Gaussian laser pulse ($\lambda = 800$ nm, $I = 1.25 \times 10^{11}$ W/cm^2, and $FWHM = 500$ μm) over a 100-μm iron slab. For the simulation, we will use a 100×100 coarse mesh with two refinement levels with a refinement ratio of two in a 1.2×0.4 mm domain. The time step employed has been $\Delta t = 10$ ps. The solvers used to solve the transport and diffusion equations are the same with those in the preceding section.

The temperature and density results obtained for a two-AMR-level simulation can be seen in Fig. 9. In Fig. 10, the relative acceleration for different refinement levels and S_n orders is shown, where it can be observed, as said previously, that the performance of TSA improves when the S_n order is decreased. It should be noted that adding new refinement levels makes the TSA have a better relative acceleration versus DSA. The reason is the better performance of TSA when the meshes have a bigger refinement, such as those presented in the finest levels of the resolution.

Finally, we have mixed both methods in an AMR simulation. The DSA has been used just to solve the coarse mesh of level 0 and TSA for the rest of the fine meshes (levels 1 and 2). We have simulated the iron plasma case for different S_n orders with two AMR levels. The resulting execution times for 1 ns (100 time steps) for this hybrid method in comparison with those obtained just using TSA and DSA are shown in Table IV. From the results, it can be inferred that using both methods is a very effective solution, showing an execution time much smaller than the simulations using TSA or DSA separately. The reason for that is that using DSA in coarse meshes and TSA in fine ones takes the advantages of the properties of both methods.

TABLE IV
EXECUTION TIMES (IN SECONDS) FOR DSA, TSA, AND HYBRID METHODS

	DSA	TSA	Hybrid
S_{14}	1985	1976	1415
S_{10}	1372	1230	951
S_6	915	795	590

VI. CONCLUSION

Two methods, namely, DSA and TSA, have been studied and compared. DSA has been shown to have, in general, a better performance than TSA, logical consequence of the fact that a diffusion equation is, in general, much easier to solve than a discrete-ordinate one. DSA has shown this advantage specially in cases with high value of ξ (when acceleration is more needed), high S_n order, and small refinement. However, TSA has shown a good performance for low S_n and high refinement problems. In the light of the results presented, we conclude that TSA can be a good candidate to be used in the resolution of the finer levels in an AMR scheme.

APPENDIX
FOURIER ANALYSIS OF THE METHODS

A) SI Method: The Fourier analysis of the iterative methods will be carried out for a stationary 2-D case, in discrete ordinates, using diamond differencing as a spatial discretization and a backward Euler time differencing in a Cartesian homogeneous mesh. Under these conditions, (6) can be written as follows in each discrete-ordinate direction m with cosines μ_m and η_m and using a level symmetric quadrature:

$$\frac{\mu_m}{\Delta x}\left(I^{l+1/2}_{m,i+1/2,j} - I^{l+1/2}_{m,i-1/2,j}\right) + \frac{\eta_m}{\Delta y}\left(I^{l+1/2}_{m,i,j+1/2} - I^{l+1/2}_{m,i,j-1/2}\right) + \sigma_{t,i,j} I^{l+1/2}_{m,i,j} = \chi_{i,j}\eta_{i,j}\sigma_{t,i,j}\phi^{l}_{i,j} + S_{i,j} \quad (18)$$

where, for simplicity, we have suppressed the g multigroup subscript and normalized the sum of the quadrature weights to the unity. The following expressions must be fulfilled, according to our assumptions:

$$I^{l+1/2}_{m,i,j} = \frac{1}{2}\left(I^{l+1/2}_{m,i+1/2,j} + I^{l+1/2}_{m,i-1/2,j}\right) \quad (19)$$

$$I^{l+1/2}_{m,i,j} = \frac{1}{2}\left(I^{l+1/2}_{m,i,j+1/2} + I^{l+1/2}_{m,i,j-1/2}\right) \quad (20)$$

$$\phi^{l+1/2}_{i,j} = \sum_{m=1}^{N} w_m I^{l+1/2}_{m,i,j} \quad (21)$$

$$\phi^{l+1} = \phi^{l+1/2}. \quad (22)$$

To do the Fourier analysis, the variables of the equation are expressed as a Fourier series, obtaining

$$\phi^{l}_{i,j}(x) = \omega^l e^{i\sigma_t(\lambda_x x_i + \lambda_y y_j)} \quad (23)$$

$$I^{l+1/2}_{m,i,j}(x) = \omega^l \alpha_m e^{i\sigma_t(\lambda_x x_i + \lambda_y y_j)} \quad (24)$$

$$I^{l+1/2}_{m,i+1/2,j}(x) = \omega^l \gamma_m e^{i\sigma_t(\lambda_x x_{i+1/2} + \lambda_y y_j)} \quad (25)$$

$$I^{l+1/2}_{m,i,j+1/2}(x) = \omega^l \delta_m e^{i\sigma_t(\lambda_x x_i + \lambda_y y_{j+1/2})} \quad (26)$$

$$\phi^{l+1/2}_{i,j}(x) = \omega^l B e^{i\sigma_t(\lambda_x x_i + \lambda_y y_j)} \quad (27)$$

where λ_x and λ_y are the Fourier modes of the series. Substituting these expressions in (19)–(22), the following equations are obtained:

$$2i\frac{\mu_m}{\Delta x}\sin\left(\frac{\sigma_t\Delta x\lambda_x}{2}\right)\gamma_m + 2i\frac{\eta_m}{\Delta y}\sin\left(\frac{\sigma_t\Delta y\lambda_y}{2}\right)\gamma_m + \sigma_t\alpha_m = \chi\eta\sigma_t \tag{28}$$

$$\alpha_m = \gamma_m\cos\left(\frac{\sigma_t\Delta x\lambda_x}{2}\right) \tag{29}$$

$$\alpha_m = \delta_m\cos\left(\frac{\sigma_t\Delta y\lambda_y}{2}\right) \tag{30}$$

$$B = \sum_{m=1}^{N} w_m\alpha_m. \tag{31}$$

After some algebra simplification, the iteration eigenvalue ω_{SI} can be expressed

$$\omega_{\mathrm{SI}} = B = \xi\sum_{m=1}^{N}\frac{w_m}{1+(\mu_m\Lambda_x+\eta_m\Lambda_y)^2} \tag{32}$$

where

$$\Lambda_x = \frac{2}{\sigma_t\Delta x}\tan\left(\frac{\sigma_t\Delta x\lambda_x}{2}\right) \tag{33}$$

$$\Lambda_y = \frac{2}{\sigma_t\Delta y}\tan\left(\frac{\sigma_t\Delta y\lambda_y}{2}\right). \tag{34}$$

B) DSA Method: In order to do the Fourier analysis of DSA, we can use the result presented in the previous section for SI method, given the fact that solving the transport equation is the first step of the method. The next step is devoted to the analysis of the diffusion equation

$$-\nabla\cdot\left(\frac{1}{3\sigma_t}\nabla R\right) + \sigma_t R = \chi\eta\sigma_t(\phi^{l+1/2}-\phi^l). \tag{35}$$

The most important aspect in dealing with this equation is the discretization of the spatial derivatives. It has been shown that a discretization inconsistent with the high-order equation can lead to a slow convergence of the method [14]. In the case of a discrete-ordinate transport equation with diamond difference, a consistent scheme is the *four-step* method, algebraically equivalent to the *source correction* proposed by Alcouffe [14] and used in PARTISN. Using this discretization, the iteration eigenvalue of the method is [13]

$$\omega_{\mathrm{DSA}} = \omega_{\mathrm{SI}} + \frac{3\xi(\omega_{\mathrm{SI}}-1)}{(\Lambda_x+\Lambda_y)^2+3(1-\xi)}. \tag{36}$$

C) TSA Method: Similar to what has been presented with TSA, to develop the Fourier analysis of TSA, the result of SI can be used, as this is the first step of the method. The analysis of the method would continue by examining the second transport equation, which we will suppose is fully converged

$$\frac{\mu_m}{\Delta x}\left(f^{l+1}_{m,i+1/2,j} - f^{l+1}_{m,i-1/2,j}\right) + \frac{\eta_m}{\Delta y}\left(f^{l+1}_{m,i,j+1/2} - f^{l+1}_{m,i,j-1/2}\right) + \sigma_t(1-\beta\eta\chi)f^{l+1}_{m,i,j} = (1-\beta)\eta\chi\sigma_t F^{l+1}_{i,j} + \eta\chi\sigma_t\left(\phi^{l+1/2}_{i,j} - \phi^l_{i,j}\right) \tag{37}$$

where

$$f^{l+1}_{m,i,j} = \frac{1}{2}\left(f^{l+1}_{m,i+1/2,j} + f^{l+1}_{m,i-1/2,j}\right) \tag{38}$$

$$f^{l+1}_{m,i,j} = \frac{1}{2}\left(f^{l+1}_{m,i,j+1/2} + f^{l+1}_{m,i,j-1/2}\right) \tag{39}$$

$$F^{l+1}_{i,j} = \sum_{m=1}^{Nlo} w_m f^{l+1}_{m,i,j} \tag{40}$$

with Nlo as the number of directions used to solve the low-order transport equation in TSA and w_m as its corresponding weights. By using the following Fourier series:

$$f^{l+1}_{m,i,j}(x) = \omega^l\alpha_m e^{i\sigma_t(\lambda_x x_i+\lambda_y y_j)} \tag{41}$$

$$f^{l+1}_{m,i,j+1/2}(x) = \omega^l\gamma_m e^{i\sigma_t(\lambda_x x_{i+1/2}+\lambda_y y_j)} \tag{42}$$

$$f^{l+1}_{m,i+1/2,j}(x) = \omega^l\delta_m e^{i\sigma_t(\lambda_x x_i+\lambda_y y_{j+1/2})} \tag{43}$$

$$F^{l+1}_{i,j}(x) = \omega^l\Gamma e^{i\sigma_t(\lambda_x x_i+\lambda_y y_j)} \tag{44}$$

and substituting in (37)–(40)

$$2i\frac{\mu_m}{\Delta x}\sin\left(\frac{\sigma_t\Delta x\lambda_x}{2}\right)\gamma_m + 2i\frac{\eta_m}{\Delta y}\sin\left(\frac{\sigma_t\Delta y\lambda_y}{2}\right)\delta_m + \sigma_t\alpha_m = (1-\beta)\eta\chi\sigma_t\Gamma + \eta\chi\sigma_t(B-1) \tag{45}$$

$$\alpha_m = \gamma_m\cos\left(\frac{\sigma_t\Delta x\lambda_x}{2}\right) \tag{46}$$

$$\alpha_m = \delta_m\cos\left(\frac{\sigma_t\Delta y\lambda_y}{2}\right) \tag{47}$$

$$\Gamma = \sum_{m=1}^{N_{lo}} w_m\alpha_m. \tag{48}$$

After some calculation efforts, we obtain

$$\Gamma = \frac{D_1(\omega_{\mathrm{SI}}-1)}{1-D_1(1-\beta)} \tag{49}$$

where D_1 is

$$D_1 = \xi\sum_{m=1}^{Nlo} w_m\frac{(1-\beta\xi)}{(1-\beta\xi)^2+(\mu_m\Lambda_x+\eta_m\Lambda_y)^2} \tag{50}$$

and the iteration eigenvalue of TSA method is

$$\omega_{\mathrm{TSA}} = \omega_{\mathrm{SI}} + \Gamma = \omega_{\mathrm{SI}} + \frac{D_1(\omega_{\mathrm{SI}}-1)}{1-D_1(1-\beta)}. \tag{51}$$

REFERENCES

[1] D. Mihalas and B. W. Mihalas, *Foundations of Radiation Hydrodynamics*. Oxford, U.K.: Oxford Univ. Press, 1984.

[2] G. C. Pomraning, *The Equations of Radiation Hydrodynamics*. Oxford, U.K.: Pergamon, 1973.

[3] E. M. Gelbard, "Spherical harmonics methods: P_L and double P_L approximations," in *Computing Methods in Reactor Physics*, H. Greenspan, C. N. Kelber, and D. Okrent, Eds. New York: Gordon & Breach, 1968.

[4] S. Chandrasekhar, *Radiative Transfer*. New York: Dover, 1960.

[5] M. González, C. García-Fernández, and P. Velarde, "2D numerical comparison between S_n and M_1 radiation transport methods," *Ann. Nucl. Energy*, vol. 36, no. 7, pp. 886–895, Jul. 2009.

[6] F. Ogando and P. Velarde, "Development of a radiation transport fluid dynamic code under AMR scheme," *J. Quant. Spectrosc. Radiat. Transf.*, vol. 71, no. 2–6, pp. 541–550, Oct. 2001.

[7] P. Velarde, D. Garcia-Senz, E. Bravo, F. Ogando, C. García, and E. Oliva, "Interaction of supernova remnants: From the circumstellar medium to the terrestrial laboratory," *Phys. Plasmas*, vol. 13, no. 9, p. 092 901, Sep. 2006.

[8] M. J. Berger and P. Colella, "Local adaptive mesh refinement for shock hydrodynamics," *J. Comput. Phys.*, vol. 82, no. 1, pp. 64–84, May 1989.

[9] R. E. Alcouffe, R. S. Baker, J. A. Dahl, S. A. Turner, and R. Ward, "PARTISN: A time-dependent, parallel neutral particle transport code system," Los Alamos Nat. Lab., Los Alamos, NM, Tech. Rep. LA-UR-08-07258, 2008.

[10] R. C. Ward, R. S. Baker, and J. E. Morel, "A diffusion synthetic acceleration method for block adaptive mesh refinement," *Nucl. Sci. Eng.*, vol. 152, no. 2, pp. 164–179, 2006.

[11] R. E. Alcouffe, B. A. Clark, and E. W. Larsen, "The diffusion-synthetic acceleration of transport iterations, with application to a radiation hydrodynamics problem," in *Multiple Time Scales*. Orlando, FL: Academic Press, 1985, pp. 73–111.

[12] E. W. Larsen, "A grey transport acceleration method for time-dependent radiative transfer problems," *J. Comput. Phys.*, vol. 78, pp. 459–480, Oct. 1988.

[13] M. L. Adams and E. W. Larsen, "Fast iterative methods for discrete-ordinates particle transport calculations," *Prog. in Nucl. Ener.*, vol. 40, no. 1, pp. 3–159, 2002.

[14] R. E. Alcouffe, "Diffusion synthetic acceleration method for the diamond-differenced discrete-ordinates equations," *Nucl. Sci. Eng.*, vol. 64, pp. 344–355, 1977.

[15] J. S. Warsa, T. A. Wareing, and J. E. Morel, "Krylov iterative methods and the degraded effectiveness of diffusion synthetic acceleration for multidimensional S–N calculations in problems with material discontinuities," *Nucl. Sci. Eng.*, vol. 147, pp. 218–248, 2004.

[16] G. L. Ramone, M. L. Adams, and P. F. Nowak, "A transport synthetic acceleration method for transport iterations," *Nucl. Sci. Eng.*, vol. 125, pp. 257–283, 1997.

[17] E. W. Larsen and W. F. Miller, "A two-step acceleration method for transport problems," *Trans. Am. Nuc. Soc.*, vol. 52, p. 416, 1986.

[18] E. Oliva, P. Zeitoun, S. Sebban, M. Fajardo, P. Velarde, K. Cassou, and D. Ros, "Optimization of soft X-ray amplifier by tailoring plasma hydrodynamics," *Opt. Lett.*, vol. 34, no. 17, pp. 2640–2642, Sep. 2009.

Carlos García-Fernández was born in 1982. He received the M.S. degree in industrial engineering (specialization in nuclear engineering) from the Universidad Politécnica de Madrid (UPM), Madrid, Spain, in 2005, where he is currently working toward the Ph.D. degree in the Instituto de Fusion Nuclear.

He is also a Research Assistant with the Instituto de Fusion Nuclear, UPM. His current research lines are radiation transport, numerical methods in AMR, and opacities.

Pedro Velarde received the M.S. degree in industrial engineering and the Ph.D. degree in nuclear engineering from the Universidad Politécnica de Madrid (UPM), Madrid, Spain, in 1987 and 1990, respectively.

He has been an Assistant Professor with the Physics Department, UPM. In 1991, he joined the Instituto de Fusion Nuclear and the Nuclear Engineering Department, UPM, where he is currently a Professor. His research interests include the hydrodynamics of high-energy density fluids, numerical methods with AMR, target design for inertial confinement fusion, laboratory astrophysics, and X-ray lasers.

Manuel Cotelo was born in 1985. He received the M.S. degree in industrial engineering (specialized in nuclear engineering) from Universidad Politécnica de Madrid (UPM), Madrid, Spain, in 2009.

He is currently a Research Assistant with the Instituto de Fusion Nuclear, UPM. His research interests include EOS, molecular dynamics, and properties of hot dense matter.